Eocene greenhouse climate revealed by coupled clumped isotope-Mg/Ca thermometry

David Evans[a,1,2], Navjit Sagoo[a], Willem Renema[b], Laura J. Cotton[b,c,d], Wolfgang Müller[e,f], Jonathan A. Todd[g], Pratul Kumar Saraswati[h], Peter Stassen[i,j], Martin Ziegler[k], Paul N. Pearson[l], Paul J. Valdes[m,n], and Hagit P. Affek[a,o]

[a]Department of Geology & Geophysics, Yale University, New Haven, CT 06511; [b]Naturalis Biodiversity Center, 2300 RA Leiden, The Netherlands; [c]Florida Museum of Natural History, University of Florida, Gainesville, FL 32611; [d]Department of Geosciences, University of Florida, Gainesville, FL 32611; [e]Institute of Geosciences, Goethe University Frankfurt, 60438 Frankfurt, Germany; [f]Department of Earth Sciences, Royal Holloway University of London, Egham, TW20 0EX, United Kingdom; [g]Department of Earth Sciences, Natural History Museum, London, SW7 5BD, United Kingdom; [h]Department of Earth Sciences, Indian Institute of Technology Bombay, Mumbai 400076, India; [i]Department of Earth and Environmental Sciences, Katholieke Universiteit Leuven, B-3000 Leuven, Belgium; [j]Royal Belgian Institute of Natural Sciences, B-1000 Brussels, Belgium; [k]Department of Earth Sciences, Utrecht University, 3584 CS Utrecht, The Netherlands; [l]School of Earth & Ocean Sciences, Cardiff University, Cardiff, CF10 3AT, United Kingdom; [m]Cabot Institute, University of Bristol, Bristol, BS8 1UJ, United Kingdom; [n]School of Geographical Sciences, University of Bristol, Bristol, BS8 1SS, United Kingdom; and [o]Institute of Earth Sciences, The Hebrew University of Jerusalem, Jerusalem 91904, Israel

Edited by Mark H. Thiemens, University of California, San Diego, La Jolla, CA, and approved December 15, 2017 (received for review August 21, 2017)

Past greenhouse periods with elevated atmospheric CO_2 were characterized by globally warmer sea-surface temperatures (SST). However, the extent to which the high latitudes warmed to a greater degree than the tropics (polar amplification) remains poorly constrained, in particular because there are only a few temperature reconstructions from the tropics. Consequently, the relationship between increased CO_2, the degree of tropical warming, and the resulting latitudinal SST gradient is not well known. Here, we present coupled clumped isotope (Δ_{47})-Mg/Ca measurements of foraminifera from a set of globally distributed sites in the tropics and midlatitudes. Δ_{47} is insensitive to seawater chemistry and therefore provides a robust constraint on tropical SST. Crucially, coupling these data with Mg/Ca measurements allows the precise reconstruction of Mg/Ca_{sw} throughout the Eocene, enabling the reinterpretation of all planktonic foraminifera Mg/Ca data. The combined dataset constrains the range in Eocene tropical SST to 30–36 °C (from sites in all basins). We compare these accurate tropical SST to deep-ocean temperatures, serving as a minimum constraint on high-latitude SST. This results in a robust conservative reconstruction of the early Eocene latitudinal gradient, which was reduced by at least 32 ± 10% compared with present day, demonstrating greater polar amplification than captured by most climate models.

clumped isotope | Eocene | tropical sea-surface temperatures | polar amplification | seawater Mg/Ca

Greenhouse periods in the geological past have received much attention as indicators of the response of the Earth to elevated CO_2. Of these, the Eocene is the most recent epoch characterized by pCO_2 at least twice preindustrial, i.e., >560 ppm (1). Furthermore, as the quantity of paleoclimate reconstructions have increased the Eocene has become a target for comparison with climate models (2), as proxy data of past warm periods are required to assess model competence at elevated CO_2 (3). Existing geochemical proxy data suggest that the Eocene latitudinal sea-surface temperature (SST) gradient was greatly reduced: the mid to high latitude (>40°) surface oceans were 10–25 °C warmer than today throughout the Eocene (4, 5), yet there is no evidence for tropical SST warming of a similar magnitude, even during peak warm intervals such as the Paleocene–Eocene Thermal Maximum (PETM) (6, 7). In fact, several studies have reported moderate tropical warmth (30–34 °C) throughout the Eocene (8, 9). This is in contrast to most Eocene climate model simulations (10, 11), which indicate the latitudinal gradient was within 20% of modern [with notable exceptions (12), discussed below]. However, using proxies to validate model output is problematic because many paleothermometers are associated with relatively large (often systematic) errors and are sensitive to diagenetic alteration after burial in the sediment. For example, initial reconstructions of the Eocene tropics were biased by the analysis of poorly preserved material, resulting in the cool-tropics hypothesis (13). Subsequently, it was shown that well-preserved samples yield Eocene tropical SST at least as warm as present (14–16). Furthermore, carbonate-bound proxies such as foraminiferal $\delta^{18}O$ and Mg/Ca are highly sensitive to poorly constrained secular variations in salinity and seawater chemistry (17), TEX_{86} is associated with calibration complications (18, 19), and all proxies may be seasonally biased to summer temperatures at mid to high latitudes (20). As a result, absolute tropical SST are not constrained to better than ±~5 °C at any given site (21), in part due to uncertainties over whether modern calibrations are applicable to Eocene material (20). Similarly, atmospheric processes, in particular clouds and aerosol–cloud interactions, are a large source of uncertainty within climate models (22), while variable intermodel sensitivities to CO_2 (10) complicate the use of these to directly constrain absolute Eocene temperatures. Given these uncertainties in both the data and models, there is no consensus regarding the degree of polar amplification or the precise response of the tropical oceans to increasing CO_2. Specifically, much debate has focused on whether the tropics underwent substantial warming and the latitudinal gradient was only moderately reduced (23, 24), or if tropical warmth was limited and the gradient

Significance

Reconstructing the degree of warming during geological periods of elevated CO_2 provides a way of testing our understanding of the Earth system and the accuracy of climate models. We present accurate estimates of tropical sea-surface temperatures (SST) and seawater chemistry during the Eocene (56–34 Ma before present, CO_2 >560 ppm). This latter dataset enables us to reinterpret a large amount of existing proxy data. We find that tropical SST are characterized by a modest warming in response to CO_2. Coupling these data to a conservative estimate of high-latitude warming demonstrates that most climate simulations do not capture the degree of Eocene polar amplification.

Author contributions: D.E., N.S., and H.P.A. designed research; D.E. performed research; D.E. analyzed data; D.E., W.R., L.J.C., J.A.T., P.K.S., P.S., and P.N.P. collected samples; H.P.A. directed clumped isotope analysis; W.M. directed laser ablation analysis; and D.E., N.S., W.R., L.J.C., W.M., J.A.T., P.K.S., P.S., M.Z., P.N.P., P.J.V., and H.P.A. wrote the paper.

The authors declare no conflict of interest.

This article is a PNAS Direct Submission.

[1]Present address: School of Earth and Environmental Sciences, University of St Andrews, St Andrews, KY16 9AL, United Kingdom.

[2]To whom correspondence should be addressed. Email: de32@st-andrews.ac.uk.

This article contains supporting information online at www.pnas.org/lookup/suppl/doi:10.1073/pnas.1714744115/-/DCSupplemental.

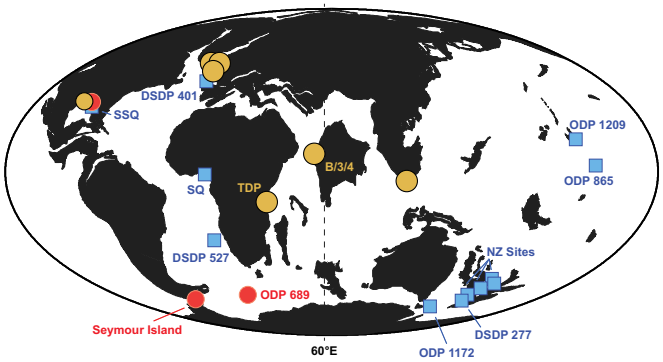

Fig. 1. Sample sites overlain on early Eocene paleogeography (created using www.odsn.de/odsn/services/paleomap/paleomap.html, after ref. 55). Yellow circles, this study (Δ_{47} and Mg/Ca); red circles, previous Δ_{47} reconstructions; blue squares, published Eocene Mg/Ca data reinterpreted here using the seawater Mg/Ca reconstruction of this study. Sites without labels are terrestrial outcrops (*SI Appendix*, Table S2).

was far lower than today (9, 25). Hence, improved reconstructions, especially in the tropics, are of fundamental importance in understanding both the response of SST to increased CO_2 as well as the accuracy of climate models. We address these issues through coupled clumped isotope-Mg/Ca measurements of shallow-dwelling large benthic foraminifera (LBF) of the family Nummulitidae. Our fossil samples come from seven globally distributed sites, four of which are in the tropics, including the equatorial West Pacific/Indian Ocean (Fig. 1). To expand this dataset to produce a global picture of Eocene tropical climate, we also derive a precise Eocene seawater Mg/Ca curve and use it to reinterpret all published Mg/Ca data from an additional 12 sites (Fig. 2).

Eocene Surface Ocean Temperature from Foraminifera Clumped Isotopes

The carbonate clumped isotope thermometer (26, 27), hereafter denoted Δ_{47}, is based on the increasingly preferential binding of heavy isotopes to each other (e.g., ^{13}C-^{18}O in carbonate) at lower temperatures. The principal advantage over existing geochemical temperature proxies is that there is no resolvable dependence on seawater elemental or isotopic composition (28), and uncertainty is dominated by analytical noise so that, unlike other carbonate-bound proxies, paleotemperature errors are random rather than systematic.

The epifaunal foraminifera utilized here live at approximately the same depth as planktonic species considered to be surface dwelling (29) (<50 m, within 1 °C of SST in the tropics; *SI Appendix*, Fig. S6), and calcify at a constant rate in locations characterized by a large seasonal cycle (30). Therefore, our paleotemperatures reflect mean annual SST. The abundance of the nummulitids in the Eocene tropics and midlatitudes, where they are rock-forming in some locations, demonstrates that they were well-adapted to the climate at the time. Three LBF species live-collected from seven locations are characterized by a Δ_{47}-temperature slope within error of the Yale abiogenic calcite calibration (27) (*SI Appendix*, Fig. S1 and Table S1), and there is no evidence for a significant vital effect influence on shell $\delta^{18}O$. These observations provide the basis for the use of this calibration to reconstruct paleotemperatures from extinct LBF of the same family.

All fossil samples were analyzed by laser-ablation inductively coupled plasma mass spectrometry (ICPMS) for a suite of trace elements to assess their geochemical preservation, together with SEM images (*SI Appendix*, Fig. S4 and Table S3). Trace element ratios indicative of contamination and overgrowths (Al/Ca and Mn/Ca) show no correlation with Mg/Ca, indicating the absence of any Mg-bearing secondary phase. SEM images of broken specimens show that Eocene and modern foraminifera are characterized by equivalent chamber wall microtextures, demonstrating the absence of micrometer-scale recrystallization. Furthermore, high-Mg calcite, such as that of LBF shells, recrystallizes fully to low-Mg, low-Sr calcite during diagenesis (*SI Appendix*, Fig. S5), enabling the unambiguous identification of geochemically well-preserved material. On the basis of these screening techniques, only samples that were exceptionally well-preserved were utilized for Δ_{47} analysis, i.e., those with no discernible diagenetic modification. Finally, because these foraminifera live at shallow depths, there is no potential for a large difference between calcification and diagenetic temperature, unlike tropical planktonic species (15).

The mean tropical SST derived from samples that passed this rigorous screening is 32.5 ± 2.5 °C (Fig. 3*A*). The maximum reconstructed Eocene Δ_{47} temperature is 36.3 ± 1.9 °C from Java at ∼39 Ma (all uncertainties are 1 SE), with a paleolatitude of 6°S (30), possibly located within an expanded Indo-Pacific warm pool. Samples spanning the early Eocene (55.3–49.9 Ma) from Kutch, India, which was within 5° of the equator at that time, are characterized by temperatures of 30.4 ± 2.5 to 35.1 ± 2.6 °C. The difficulty in precise temporal correlation between shallow sites means that we cannot definitively assign these samples to specific intervals, although the youngest and warmest Kutch sample probably falls within the Early Eocene Climatic Optimum (EECO; ∼52–50 Ma). Although the peak temperature from equatorial India in the early Eocene is marginally cooler than that from middle Eocene Java, the two are within error, and this small difference may be explained by regionally cooler SST on the west coast of India compared with the West Pacific. A latest Eocene sample from Tanzania (33.9 Ma; 21°S) records 29.7 ± 3.1 °C.

In addition, samples spanning the early–middle Eocene from northwest Europe were analyzed for Δ_{47} and Mg/Ca. The principal aim of doing so was to fill temporal gaps in our seawater chemistry reconstructions (see below), but these also provide Eocene SST for this region. We observe a 9 °C warming between the earliest Eocene (18–20 °C) and the EECO (28–31 °C), followed by a long-term cooling trend through the Mid-Eocene to 23.1 ± 2.5 °C at 42.5 Ma. This pattern of global change is in good agreement with mid- to high-latitude TEX_{86} (31) (*SI Appendix*, Fig. S8).

Finally, calculated $\delta^{18}O_{sw}$, derived from $\delta^{18}O_c$ measured simultaneously with Δ_{47}, yield values that are in agreement with an ice-free world. Specifically, all $\delta^{18}O_{sw}$ reconstructions from our tropical samples are within error of −1‰, with the exception of

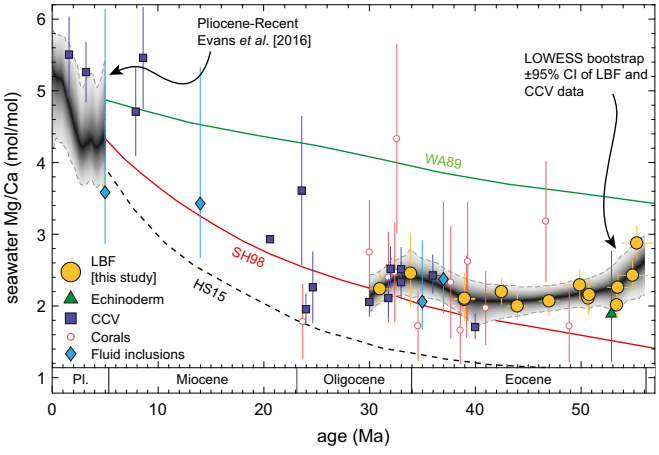

Fig. 2. Seawater Mg/Ca reconstruction for the Eocene and early Oligocene based on coupled Δ_{47}-Mg/Ca LBF and ridge-flank $CaCO_3$ vein (CCV) data, shown in the context of previous Cenozoic reconstructions (33, 34, 56, 57) and box models (refs. 35, 36, and 58; WA89, SH98, and HS15, respectively), that are commonly used for calculating planktonic and deep-benthic foraminifera Mg/Ca data. Coral-derived data younger than 20 Ma are omitted. The 95% confidence intervals on our Eocene Mg/Ca_{sw} curve are derived from bootstrapping 1,000 locally weighted scatterplot smoothing (LOWESS) fits, including both geochemical and dating uncertainties.

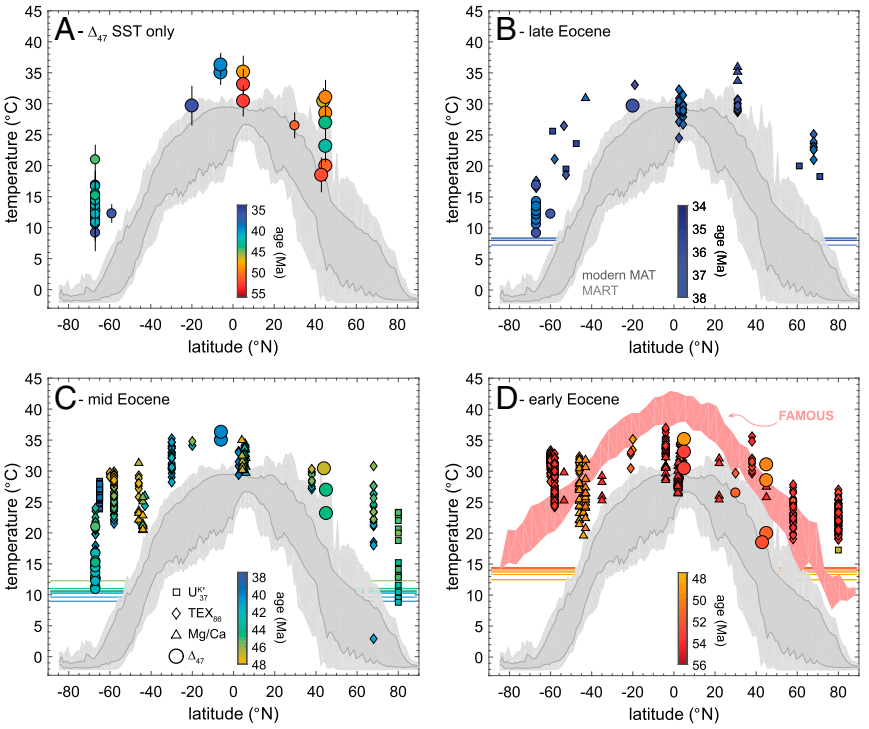

Fig. 3. Eocene clumped isotope SST reconstruction and reevaluated Mg/Ca temperatures (this study) shown in the context of organic proxies. (*A*) All clumped isotope-derived SST. Smaller symbols are previously published data. (*B–D*) Eocene SST proxy data, split into three time intervals (34–38, 38–48, and 48–56 Ma). All Mg/Ca data were reevaluated based on our Mg/Ca_{sw} curve (Fig. 2). TEX_{86} temperatures were recalculated using the TEX_{86}^{H} calibration (59). See *SI Appendix* for references. Horizontal lines show Eocene Mg/Ca-derived deep-ocean temperatures (44). The modern mean annual temperature (MAT) and seasonal range in SST (MART) are depicted by dark- and light-gray shading, respectively. Marker and line color depict sample age; note the color scale is the same in all panels. Data are compared with an Eocene GCM simulation [FAMOUS model E17 (46) at 560 ppm CO_2] in *D*.

Tanzania (−0.2‰). $\delta^{18}O_{sw}$ at our midlatitude sites is temporally variable and characterized by overall more negative values, consistent with midlatitude freshwater contribution to these proximal sites (−4 to −1.5‰). These data further demonstrate that our samples are well-preserved, and that the sample site salinity was not substantially lower than open ocean (all $\delta^{18}O_{sw}$ within 3‰ of mean Eocene seawater). Because a >10-psu salinity reduction is necessary to significantly change seawater Mg/Ca (Mg/Ca_{sw}), our LBF Mg/Ca data discussed below must also represent normal seawater conditions (*SI Appendix*, Fig. S7).

Our samples do not include the PETM, and only one falls within the EECO. Therefore, our results do not preclude warmer tropical temperatures during those time intervals (6). Nonetheless, we find no evidence for tropical SST >38 °C based on our Δ_{47} data. Indeed, all of our tropical data are within uncertainty of each other, and could be interpreted as indicating stable warm conditions in the tropics throughout the Eocene (32.5 ± 2.5 °C), in line with several previous studies (8, 14, 32), although possible temporal trends will be discussed below. To assess whether a similar picture is evident in other proxy SST data, and therefore to address the broader questions of the Eocene evolution of tropical SST and early Eocene polar amplification, we use these Δ_{47} paleotemperatures, together with Mg/Ca analyses of the same samples, to accurately and precisely reconstruct Mg/Ca_{sw}. This allows us to reevaluate all Eocene planktonic foraminifera Mg/Ca data, providing an additional constraint on tropical SST at higher temporal and spatial resolution than the Δ_{47} data alone. Furthermore, by combining information from these proxies we create a large dataset consisting mostly of open ocean data, suitable for comparison with climate simulations. Doing so minimizes potential bias associated with the regional paleoceanography of any individual site.

Seawater Mg/Ca Reconstruction

Coupling Mg/Ca-Δ_{47} data of the same specimens allows us to simultaneously reconstruct temperature and Mg/Ca_{sw} because shell Mg/Ca is a function of both, and we independently constrain the temperature component of Mg incorporation using Δ_{47}. Although much work has focused on reconstructing past variation in Mg/Ca_{sw} (33, 34), a different approach is required. While these studies show that Mg/Ca_{sw} has approximately doubled since the Oligocene (35), precise reconstructions for most of the Paleogene are lacking, and models covering the Phanerozoic (35, 36) do not agree on epoch-scale variation in seawater chemistry. This has precluded reliable Mg/Ca-derived paleotemperatures with sufficient accuracy for assessing model SST competency (17). To overcome this, we use Δ_{47} data of LBF spanning the Eocene–early Oligocene to solve the Mg/Ca_{LBF}–Mg/Ca_{sw}-temperature calibration for these foraminifera (37). The uncertainty in these reconstructions is ∼2–5× lower than previous estimates, reducing the Mg/Ca_{sw}-derived error on existing planktonic foraminifera temperatures to <2.5 °C. This is possible because nummulitid Mg/Ca is more sensitive to Mg/Ca_{sw} than to temperature, and unlike planktonic species there are no resolvable salinity or carbonate chemistry effects (30, 37). The composite Paleogene Mg/Ca_{sw} curve (Fig. 2) is based on our LBF and data from inorganic calcium carbonate veins (CCV) (33), as the uncertainty on these latter data is also relatively small and the two records are in excellent agreement where they overlap. This reconstruction delineates the Eocene–early Oligocene as a period of stable Mg/Ca_{sw} between 2.1 and 2.5 mol mol^{-1}, ∼45% of modern. Previously, the lack of data before 40 Ma required box-model estimates (35, 36) to be used to assess the impact of secular change in seawater chemistry on fossil Mg/Ca measurements. The precise LBF-derived Mg/Ca_{sw} data (Fig. 2) demonstrate that those models are inaccurate in the early Eocene, with a large effect on Mg/Ca-derived temperatures. For example, early Eocene tropical SST

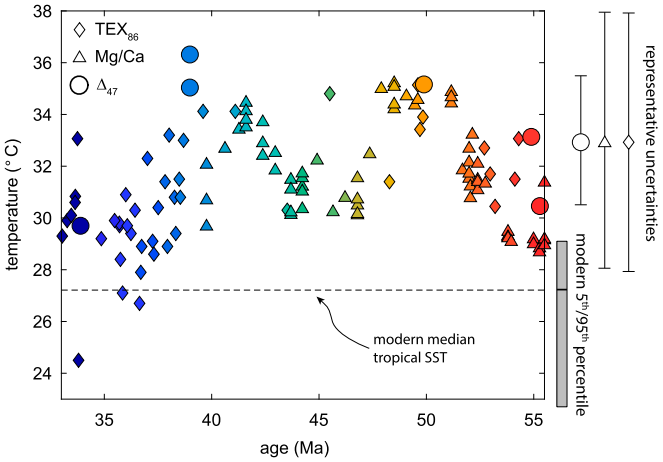

Fig. 4. Evolution of tropical (<23°) SST through the Eocene. Note that scatter in the proxy data is of a similar magnitude as the modern range in tropical SST (gray bar). Representative errors are 1 SE for Δ_{47}, propagated uncertainties derived from the influence of Mg/Ca_{sw} and pH on Mg/Ca, and 2 SE for TEX_{86}. The modern median and 95th percentiles are based on the World Ocean Atlas (*SI Appendix*).

calculated using our Mg/Ca_{sw} would result in temperatures 6–10 °C cooler compared with the model output of ref. 35, yet warmer by a similar magnitude using the model of ref. 36.

Eocene Tropical Warmth

In light of both our tropical clumped isotope data and revised planktonic foraminifera Mg/Ca temperatures utilizing the precise Mg/Ca_{sw} reconstruction described above, we are able to estimate low-latitude SST across the globe and throughout the Eocene, thus placing constraints on the early-Eocene latitudinal gradient (Figs. 3 and 4). When doing so it must be considered that in addition to Mg/Ca_{sw}, both salinity and the carbonate system may bias planktonic foraminifera Mg/Ca-derived SST (21, 38). We consider the impact of pH in detail (*SI Appendix*), but do not apply a salinity correction because mean Eocene ocean salinity was similar to today (39). Although Mg/Ca and TEX_{86} are associated with relatively large uncertainties (~±3–5 °C) related to nonthermal influences and calibration complications, Δ_{47}, reinterpreted planktonic Mg/Ca, and TEX_{86} are in good agreement in the tropics. This indicates that if either is systematically offset in this region, it is by less than the magnitude of the stated error, lending support to the interpretation of Eocene GDGTs in terms of SST in the tropics (cf. refs. 19 and 40).

The tropical compilation constrains SST to between 30 and 36 °C throughout the Eocene (Fig. 4), with the exception of late Eocene TEX_{86} from Ocean Drilling Program (ODP) Site 929/925 (31) which range between 27 and 32 °C, and the earliest Eocene Mg/Ca data from ODP Site 865 (26–31 °C). Although the Δ_{47} reconstructions from the middle Eocene of Java are 1 °C higher than the EECO of Kutch, this may simply reflect zonal differences in Eocene tropical SST, which is likely given that the modern tropics are characterized by similar zonal SST variability (Fig. 4). Additionally, the compilation highlights that the 2–5 °C tropical warming between the earliest Eocene and the EECO shown by the Δ_{47} data from Kutch is in good agreement with planktonic foraminifera Mg/Ca from ODP Site 865 (recalculated from ref. 41) and earliest Eocene TEX_{86} data (6); early Eocene equatorial clumped isotope temperatures of 30–33 °C are therefore not anomalously cool.

These data do not rule out the possibility of higher temperatures over transient events such as the PETM (6), and therefore do not constrain peak Eocene tropical warmth. They do provide strong evidence that the early Eocene tropical oceans in general were not warmer than 36 °C (mean ~33 °C, upper uncertainty 38 °C), unless all proxies are biased toward lower temperatures. Given that there is no reason to suspect this, our data provide a well-constrained basis to examine the early Eocene latitudinal gradient and the accuracy of Eocene model simulations.

Early Eocene Latitudinal SST Gradient

To use our tropical SST compilation to quantitatively constrain the equator-pole SST gradient for the early Eocene (the interval to which most model simulations are compared), we first review the high-latitude proxy data. Eocene SST derived from TEX_{86} data from the Arctic Coring Expedition (ACEX) (42) (~80°N), ODP Site 1172 (5) (~54°S), and Wilkes Land (43) (~60°S) greatly exceed deep-ocean temperatures derived from deep-benthic foraminifera Mg/Ca and $\delta^{18}O$ (44), suggesting either a seasonal bias, the influence of local warm surface currents, a more stratified ocean, and/or uncertain calibrations (20). To avoid these complications, we use the deep-benthic foraminifera-Mg/Ca temperature stack (44) as a lower limit on high-latitude SST. Present-day mean SST at high latitudes is within 2 °C of the deep ocean (*SI Appendix*), and the coolest Eocene high-latitude Δ_{47} data based on long-lived shallow benthic molluscs from Seymour Island (45) are within error of coeval deep-ocean temperatures where both are available (Fig. 3 *B* and *C*). Although the coherence of these reconstructions supports the use of deep-ocean Mg/Ca as a minimum constraint on high-latitude SST through time, model evidence suggests that Eocene deep-water formation in the Southern Ocean may have been limited to winter (20), resulting in colder deep water compared with mean annual high-latitude SST. Therefore, we emphasize that using the benthic foraminifera Mg/Ca dataset as a proxy for high-latitude SST produces an estimate of the maximum steepness of the latitudinal SST gradient and does not necessarily represent the mean annual gradient. Similarly, it does not in itself provide a means of assessing high-latitude SST proxy data given that these may be biased toward a different season, and there is evidence for a zonal SST heterogeneity in the Eocene Southern Ocean (45). The merit in this approach is that it provides a conservative constraint on the degree to which the gradient was reduced in the Eocene, and therefore represents the minimum that model simulations must achieve to be considered representative of Eocene climate. We calculate the early Eocene latitudinal gradient as the difference between the mean tropical and deep-ocean data between 48 and 56 Ma (±2-SE variability in both datasets); it is therefore representative of background early Eocene conditions [i.e., not the PETM, for which there is evidence for a further reduction in the latitudinal SST gradient (21)].

Based on this analysis, we find a reduction of at least 32 ± 10% in the mean difference between tropical and high-latitude SST during the early Eocene (48–56 Ma), relative to present day (Fig. 5*A*). The quantity (n = 123) and coherence of tropical early Eocene data from Δ_{47} and two other proxies means that we can confidently use this as a conservative estimate to assess model competency. Splitting the early Eocene into intervals approximating the EECO (50–52.5 Ma) versus post-PETM, pre-EECO (55–52.5 Ma) does not significantly alter our finding as the latitudinal gradient for both intervals is within the uncertainty of the early Eocene data overall. Therefore, for the purposes of model-data comparison we do not split the early Eocene in this way because the overall sparsity of data may result in a regionally biased comparison.

Eocene Model-Data Comparison

Polar amplification in climate models of past warm periods has received much attention as it has long been suggested that simulations may not capture the extent to which the latitudinal SST gradient is reduced. In the Eocene, this debate has focused in part on the magnitude of tropical warming (23). For example, if tropical SST were far higher than at present and if high-latitude proxy data were summer-biased, then some models would be in overall agreement with the data (20). Our Δ_{47} reconstructions and SST compilation (Figs. 3 and 4) demonstrate that early Eocene tropical warming was of a substantially lower magnitude than in most models, and therefore indicate that the proxy data are irreconcilable with these simulations even when accounting for complicating factors in the high latitudes. Other simulations indicate SST exceeding the proxy estimates in both the tropics and high latitudes. For

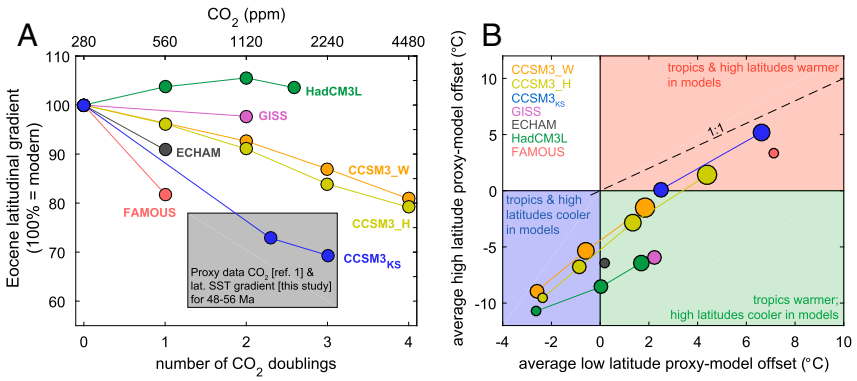

Fig. 5. Early Eocene (48–56 Ma) model-data comparison. (*A*) Zonally averaged latitudinal gradients based on proxy CO_2 and SST data (gray box) and climate models over a range of CO_2 (circles) (12, 46–48, 60). Proxy CO_2 range is from ref. 1; the gradient uncertainty is the combined 2 SE of the tropical and high-latitude proxy data (see text). Proxy-derived gradient is shown relative to present day; Eocene climate model simulations are shown relative to their preindustrial counterpart. Most model simulations do not capture the reduced latitudinal gradient within the range of proxy CO_2 (<2,250 ppm). (*B*) Site-specific model-data comparison for both the tropics and high latitudes. Model SST competency assessed by comparing the mean difference between the model and proxy data for low and high latitudes. Quadrants reflect different overall patterns of model-data offset. Hypothetical simulations falling on the 1:1 line would reconstruct the same latitudinal gradient as the data but not the same absolute SST, except at the origin. All models fall below this line, indicating that Eocene polar amplification is underestimated.

example, the FAMOUS model simulation (46) shown in the context of the early Eocene proxy data in Fig. 3*D* is notable because it produces a substantially reduced latitudinal SST gradient. However, the parameter changes used to achieve this gradient reduction result in tropical SST that are ∼7 °C warmer than the proxy data.

Extending this comparison (Fig. 5*A*) by comparing the Eocene data latitudinal gradient to a number of climate simulations shows that HadCM3L (47) and GISS (48) are characterized by SST gradients within 10% of their preindustrial simulation. In contrast, CCSM (as configured by refs. 49 and 50) approaches the proxy gradient at four CO_2 doublings (4,480 ppm), while the CCSM models of ref. 12 (hereafter $CCSM_{KS}$) and the warmest FAMOUS simulation (46) fall within the range of the proxy data, achieving latitudinal gradients below 80% of modern at 560 ppm CO_2. The common feature of these latter models is that both have substantially modified parameters related to cloud formation resulting in a reduction in low-level stratiform cloud, increased precipitation rates, and an increase in incoming shortwave radiation. Such clouds are more prevalent at high latitudes, resulting in preferential surface warming of these regions.

Although models with modified cloud properties are within error of a conservative latitudinal proxy gradient, this does not imply agreement in terms of absolute temperatures (e.g., compare FAMOUS to the data in Fig. 3*D*). Therefore, to assess the ability of models to reconstruct both absolute SST and the latitudinal gradient, and to avoid the potential bias introduced by condensing model-data comparison into a latitudinal transect, the offsets between the proxy data and the nearest model grid cells were calculated to produce a location-specific proxy-model comparison. Fig. 5*B* and *SI Appendix*, Figs. S11–S14 display the result of this exercise in terms of the average tropical and high-latitude proxy-model offset, i.e., the mean of location-specific offsets between the model and data for the two regions (as above, the high-latitude proxy-model offset was conservatively estimated based on deep-ocean temperatures; *SI Appendix*). Models with Eocene latitudinal gradients similar to present day such as HadCM3L and ECHAM (Fig. 5*A*) consistently underestimate high-latitude SST. Moreover, we find that no simulation captures our conservative estimate of the latitudinal gradient and the absolute proxy temperatures. Specifically, most models that lie close to the 1:1 line in Fig. 5*B*, representing agreement in terms of the latitudinal gradient, overestimate both tropical and high-latitude SST and require pCO_2 greater than that indicated by the proxy data. Nonetheless, three CCSM simulations fall within 2–3 °C of the origin in Fig. 5*B*, indicating that these are close to reproducing our conservative analysis of the early Eocene latitudinal gradient, as well as the absolute proxy temperatures. $CCSM_{KS}$, with modified cloud properties, achieves this with pCO_2 within the range of proxy data (1). However, we stress that our derivation of the early Eocene latitudinal gradient is conservative. If high-latitude mean annual SST were in fact warmer than the deep ocean, then the model-data comparison would be considerably less favorable. Similarly, evidence for further polar amplification during the PETM (21) predicts a less-favorable comparison. Therefore, our analysis indicates that a further mechanism of polar amplification is likely to be required to fully reconcile models with peak Eocene warmth, given that $CCSM_{KS}$ (the best-performing simulations in our analysis) is characterized by a similar latitudinal SST gradient when run under pre-PETM and PETM conditions (Fig. 5*A*).

Our coupled Δ_{47}-Mg/Ca data and subsequent reanalysis of planktonic Mg/Ca temperatures via the precise reconstruction of Mg/Ca_{sw} demonstrate that the early Eocene mean latitudinal SST gradient was at least 32 ± 10% shallower than modern. Based on a location-specific comparison that avoids latitudinal averaging, we find that few modeling efforts (12) are close to reproducing both this gradient and the absolute proxy SST. Further work is required to capture the possible additional reduction in this gradient during peak warm intervals, or if Eocene mean annual high-latitude SST were warmer than the deep ocean. The most accurate Eocene simulations with respect to SST independently achieved this by modifying aerosol and cloud properties, highlighting the importance of this research direction as a potential mechanism for polar amplification (51).

Materials and Methods

All fossil samples come from clay or sand horizons (e.g., ref. 30) and none contained noticeable carbonate infillings that may bias the data. Additionally, broken chamber wall sections of key samples were imaged by SEM to confirm that micrometer-scale recrystallization had not taken place.

Samples were analyzed by laser-ablation ICPMS using the RESOlution M-50 system at Royal Holloway University of London (RHUL) (52). The procedure for nondestructive analysis of LBF has been described in detail elsewhere (37), and was modified only in that the Agilent 7500 ICPMS used in that study was replaced with an Agilent 8800 triple-quadrupole ICPMS partway through the analytical period. Before clumped isotope measurement every specimen was analyzed by laser-ablation ICPMS to assess preservation on an individual specimen basis. The only exception to this was sample W10-3c and EF1/2, which contained abundant foraminifera, and all specimens analyzed were found to be geochemically well-preserved. Therefore, screening of every foraminifera was unnecessary. Aside from widely used preservation indicators such as Al/Ca for clay contamination and Mn/Ca for overgrowths, Mg/Ca and Sr/Ca are also useful preservation indicators as the Mg and Sr concentration of high-Mg calcite decreases upon recrystallization to values substantially lower than well-preserved Eocene LBF specimens (pervasively recrystallized samples are shown for comparison in *SI Appendix*, Fig. S5).

The clumped isotope analytical procedure at Yale University is described in detail elsewhere (45, 53). Larger specimens were crushed before cleaning; smaller specimens were analyzed as multiple whole shells. Modern samples were ultrasonicated for 30 min in ∼7% H_2O_2, rinsed three times in distilled

water, and dried under vacuum at 25 °C. Fossil samples with lower organic content were ultrasonicated in methanol followed by distilled water only to remove any clay adherents. Then ∼3–5 mg of sample was reacted overnight with 103–105% H_3PO_4 at 25 °C. The CO_2 was extracted through a H_2O trap and cleaned of volatile organic compounds using a 30-m Supelco Q-Plot GC column at −20 °C. Isotopic analyses were performed on a Thermo MAT253 optimized to measure *m/z* 44–49. Masses 48 and 49 were used to assess sample purity. Standardization was performed through the analysis of CO_2 with a range of $\delta^{18}O$ and $\delta^{13}C$, heated to 1,000 °C (termed "heated gases") and transferred into the absolute reference frame as previously described (53, 54) using standards with a Δ_{47} range that spans the samples (see *SI Appendix* for details).

ACKNOWLEDGMENTS. We thank the editor, and reviewers for their constructive comments which greatly improved this paper. D.E. and H.P.A. acknowledge support from Yale University and the Yale Analytical and Stable Isotope Center and from Grant 171/16 of the Israel Science Foundation. W.R. and L.J.C. were supported by NWO Grant ALW 822 01 009. The Tanzania Commission for Science and Technology (COSTECH) and the Tanzania Petroleum Development Corporation supported the Tanzania Drilling Project (TDP) which recovered the Tanzanian specimens. Laser-ablation ICPMS work at RHUL was partly funded by a 2014 Natural Environment Research Council (NERC) Capital Equipment Grant (Ref. CC073). The Research Foundation Flanders is acknowledged for financial support (to P.S.). M.Z. acknowledges support from the Netherlands Earth System Science Center and Horizon 2020 Grant MSCA-IF-2014 655073.

1. Anagnostou E, et al. (2016) Changing atmospheric CO_2 concentration was the primary driver of early Cenozoic climate. *Nature* 533:380–384.
2. Lunt DJ, et al. (2017) The DeepMIP contribution to PMIP4: Experimental design for model simulations of the EECO, PETM, and pre-PETM (version 1.0). *Geosci Model Dev* 10:889–901.
3. Haywood AM, et al. (2011) Are there pre-Quaternary geological analogues for a future greenhouse warming? *Philos Trans A Math Phys Eng Sci* 369:933–956.
4. Hollis CJ, et al. (2009) Tropical sea temperatures in the high-latitude South Pacific during the Eocene. *Geology* 37:99–102.
5. Bijl PK, et al. (2009) Early Palaeogene temperature evolution of the southwest Pacific Ocean. *Nature* 461:776–779.
6. Frieling J, et al. (2017) Extreme warmth and heat-stressed plankton in the tropics during the Paleocene-Eocene Thermal Maximum. *Sci Adv* 3:e1600891.
7. Aze T, et al. (2014) Extreme warming of tropical waters during the Paleocene-Eocene thermal maximum. *Geology* 42:739–742.
8. Pearson PN, et al. (2007) Stable warm tropical climate through the Eocene Epoch. *Geology* 35:211.
9. Keating-Bitonti CR, Ivany LC, Affek HP, Douglas P, Samson SD (2011) Warm, not super-hot, temperatures in the early Eocene subtropics. *Geology* 39:771–774.
10. Lunt DJ, et al. (2012) A model–data comparison for a multi-model ensemble of early Eocene atmosphere–ocean simulations: EoMIP. *Clim Past* 8:1717–1736.
11. Lunt DJ, et al. (2013) Warm climates of the past–A lesson for the future? *Philos Trans R Soc A Math Phys Eng Sci* 371:20130146.
12. Kiehl JT, Shields CA (2013) Sensitivity of the Palaeocene-Eocene Thermal maximum climate to cloud properties. *Philos Trans A Math Phys Eng Sci* 371:20130093.
13. Shackleton NJ, Boersma A (1981) The climate of the Eocene ocean. *J Geol Soc London* 138:153–157.
14. Pearson PN, et al. (2001) Warm tropical sea surface temperatures in the Late Cretaceous and Eocene epochs. *Nature* 413:481–487.
15. Schrag DP, Depaolo DJ, Richter FM (1995) Reconstructing past sea surface temperatures: Correcting for diagenesis of bulk marine carbonate. *Geochim Cosmochim Acta* 59:2265–2278.
16. Schrag DP (1999) Effects of diagenesis on the isotopic record of late Paleogene tropical sea surface temperatures. *Chem Geol* 161:215–224.
17. Evans D, Müller W (2012) Deep time foraminifera Mg/Ca paleothermometry : Nonlinear correction for secular change in seawater Mg/Ca. *Paleoceanography* 27:PA4205.
18. Tierney JE, Tingley MP (2014) A Bayesian, spatially-varying calibration model for the TEX_{86} proxy. *Geochim Cosmochim Acta* 127:83–106.
19. Ho SL, Laepple T (2016) Flat meridional temperature gradient in the early Eocene in the subsurface rather than surface ocean. *Nat Geosci* 9:606–610.
20. Hollis CJ, et al. (2012) Early Paleogene temperature history of the southwest Pacific Ocean : Reconciling proxies and models. *Earth Planet Sci Lett* 349–350:53–66.
21. Evans D, Wade BS, Henehan M, Erez J, Müller W (2016) Revisiting carbonate chemistry controls on planktic foraminifera Mg/Ca: Implications for sea surface temperature and hydrology shifts over the Paleocene-Eocene Thermal Maximum and Eocene-Oligocene transition. *Clim Past* 12:819–835.
22. Boucher O, Randall D (2013) *Clouds and Aerosols. Climate Change 2013: The Physical Science Basis* (Cambridge Univ Press, New York), pp 571–657.
23. Huber M (2008) Climate change. A hotter greenhouse? *Science* 321:353–354.
24. Williams IN, Pierrehumbert RT, Huber M (2009) Global warming, convective threshold and false thermostats. *Geophys Res Lett* 36:2–6.
25. Spicer RA, et al. (2014) Cool tropics in the Middle Eocene: Evidence from the Changchang Flora, Hainan Island, China. *Palaeogeogr Palaeoclimatol Palaeoecol* 412:1–16.
26. Ghosh P, et al. (2006) ^{13}C–^{18}O bonds in carbonate minerals: A new kind of paleothermometer. *Geochim Cosmochim Acta* 70:1439–1456.
27. Zaarur S, Affek HP, Brandon MT (2013) A revised calibration of the clumped isotope thermometer. *Earth Planet Sci Lett* 382:47–57.
28. Tang J, Dietzel M, Fernandez A, Tripati AK, Rosenheim BE (2014) Evaluation of kinetic effects on clumped isotope fractionation (Δ_{47}) during inorganic calcite precipitation. *Geochim Cosmochim Acta* 134:120–136.
29. Renema W (2006) Large benthic foraminifera from the deep photic zone of a mixed siliciclastic-carbonate shelf off East Kalimantan, Indonesia. *Mar Micropaleontol* 58:73–82.
30. Evans D, Müller W, Oron S, Renema W (2013) Eocene seasonality and seawater alkaline earth reconstruction using shallow-dwelling large benthic foraminifera. *Earth Planet Sci Lett* 381:104–115.
31. Inglis GN, et al. (2015) Descent toward the Icehouse: Eocene sea surface cooling inferred from GDGT distributions. *Paleoceanography* 30:1000–1020.
32. Kozdon R, Kelly DC, Kita NT, Fournelle JH, Valley JW (2011) Planktonic foraminiferal oxygen isotope analysis by ion microprobe technique suggests warm tropical sea surface temperatures during the Early Paleogene. *Paleoceanography* 26:PA3206.
33. Coggon RM, Teagle DA, Smith-Duque CE, Alt JC, Cooper MJ (2010) Reconstructing past seawater Mg/Ca and Sr/Ca from mid-ocean ridge flank calcium carbonate veins. *Science* 327:1114–1117.
34. Gothmann AM, et al. (2015) Fossil corals as an archive of secular variations in seawater chemistry since the Mesozoic. *Geochim Cosmochim Acta* 160:188–208.
35. Stanley SM, Hardie LA (1998) Secular oscillations in the carbonate mineralogy of reef-building and sediment-producing organisms driven by tectonically forced shifts in seawater chemistry. *Palaeogeogr Palaeoclimatol Palaeoecol* 144:3–19.
36. Wilkinson B, Algeo T (1989) Sedimentary carbonate record of calcium-magnesium cycling. *Am J Sci* 289:1158–1194.
37. Evans D, Erez J, Oron S, Müller W (2015) Mg/Ca-temperature and seawater-test chemistry relationships in the shallow-dwelling large benthic foraminifera Operculina ammonoides. *Geochim Cosmochim Acta* 148:325–342.
38. Hönisch B, et al. (2013) The influence of salinity on Mg/Ca in planktic foraminifers–Evidence from cultures, core-top sediments and complementary $\delta^{18}O$. *Geochim Cosmochim Acta* 121:196–213.
39. Hay WW, et al. (2006) Evaporites and the salinity of the ocean during the Phanerozoic: Implications for climate, ocean circulation and life. *Palaeogeogr Palaeoclimatol Palaeoecol* 240:3–46.
40. Tierney JE, Sinninghe Damsté JS, Pancost RD, Sluijs A, Zachos JC (2017) Eocene temperature gradients. *Nat Geosci* 10:538–539.
41. Tripati AK (2003) Tropical sea-surface temperature reconstruction for the early Paleogene using Mg/Ca ratios of planktonic foraminifera. *Paleoceanography* 18:1101.
42. Sluijs A, et al. (2008) Arctic late Paleocene–early Eocene paleoenvironments with special emphasis on the Paleocene-Eocene thermal maximum (Lomonosov Ridge, Integrated Ocean Drilling Program Expedition 302). *Paleoceanography* 23:PA1S11.
43. Bijl PK, et al.; Expedition 318 Scientists (2013) Eocene cooling linked to early flow across the Tasmanian Gateway. *Proc Natl Acad Sci USA* 110:9645–9650.
44. Cramer BS, Miller KG, Barrett PJ, Wright JD (2011) Late Cretaceous–Neogene trends in deep ocean temperature and continental ice volume: Reconciling records of benthic foraminiferal geochemistry ($\delta^{18}O$ and Mg/Ca) with sea level history. *J Geophys Res* 116:C12023.
45. Douglas PMJ, et al. (2014) Pronounced zonal heterogeneity in Eocene southern high-latitude sea surface temperatures. *Proc Natl Acad Sci USA* 111:6582–6587.
46. Sagoo N, Valdes P, Flecker R, Gregoire LJ (2013) The Early Eocene equable climate problem: Can perturbations of climate model parameters identify possible solutions? *Philos Trans A Math Phys Eng Sci* 371:20130123.
47. Lunt DJ, et al. (2010) CO_2-driven ocean circulation changes as an amplifier of Paleocene-Eocene thermal maximum hydrate destabilization. *Geology* 38:875–878.
48. Roberts CD, LeGrande AN, Tripati AK (2009) Climate sensitivity to Arctic seaway restriction during the early Paleogene. *Earth Planet Sci Lett* 286:576–585.
49. Huber M, Caballero R (2011) The early Eocene equable climate problem revisited. *Clim Past* 7:603–633.
50. Winguth A, Shellito C, Shields C, Winguth C (2010) Climate response at the paleocene-eocene thermal maximum to greenhouse gas forcing-a model study with CCSM3. *J Clim* 23:2562–2584.
51. Schneider T, et al. (2017) Climate goals and computing the future of clouds. *Nat Clim Chang* 7:3–5.
52. Müller W, Shelley M, Miller P, Broude S (2009) Initial performance metrics of a new custom-designed ArF excimer LA-ICPMS system coupled to a two-volume laser-ablation cell. *J Anal At Spectrom* 24:209–214.
53. Zaarur S, Affek HP, Stein M (2016) Last glacial-Holocene temperatures and hydrology of the Sea of Galilee and Hula Valley from clumped isotopes in Melanopsis shells. *Geochim Cosmochim Acta* 179:142–155.
54. Dennis KJ, Affek HP, Passey BH, Schrag DP, Eiler JM (2011) Defining an absolute reference frame for "clumped" isotope studies of CO_2. *Geochim Cosmochim Acta* 75:7117–7131.
55. Hay WW, et al. (1999) Alternative global Cretaceous paleogeography. *Evolution of the Cretaceous Ocean-Climate System*, Geological Society of America Special Paper 332, eds Barrera E, Johnson CC (Geological Society of America, Boulder, CO), pp 1–39.
56. Horita J, Zimmermann H, Holland HD (2002) Chemical evolution of seawater during the Phanerozoic. *Geochim Cosmochim Acta* 66:3733–3756.
57. Evans D, Brierley C, Raymo ME, Erez J, Müller W (2016) Planktic foraminifera shell chemistry response to seawater chemistry: Pliocene-Pleistocene seawater Mg/Ca, temperature and sea level change. *Earth Planet Sci Lett* 438:139–148.
58. Higgins JA, Schrag DP (2015) The Mg isotopic composition of Cenozoic seawater:–Evidence for a link between Mg-clays, seawater Mg/Ca, and climate. *Earth Planet Sci Lett* 416:73–81.
59. Kim J-H, et al. (2010) New indices and calibrations derived from the distribution of crenarchaeal isoprenoid tetraether lipids: Implications for past sea surface temperature reconstructions. *Geochim Cosmochim Acta* 74:4639–4654.
60. Heinemann M, Jungclaus JH, Marotzke J (2009) Warm Paleocene/Eocene climate as simulated in ECHAM5/MPI-OM. *Clim Past* 5:785–802.